

A COMPARISON OF PRECIPITATION INTENSITY FROM RADER WITH MODEL RESULTS AROUND COASTAL TOPOGRAPHY DURING COLD - AIR OUTBREAK PERIODS

Sento Nakai^{*1}, Teruyuki Kato^{*2}, Katsushi Iwamoto^{*1}, Masaaki Ishizaka^{*1}
¹ Snow and Ice Research Center, NIED
² Meteorological Research Institute, JMA

1. Introduction

The effect of topography on shallow convection is relatively large. Snow clouds, developing over the central part of the Japan Sea in winter, usually have a cloud top height of 4000 to 6000 m. The cloud top height is restricted by a low level of neutral buoyancy, brought from the low temperature of a lifted air. Such stratification results in the strong topographic effect on the convective cloud systems, influencing the snowfall distribution over the land and the occurrence possibility of snow-related disasters.

Nakai and Endoh (1995) pointed out that a convective mixed layer behaves as a shallow-water layer when it passes over a low mountain barrier of a height of 600 m and that supercooled droplets generated by orographic lifting can produce the enhancement of snowfall in the lower convective mixed layer. Partial blocking and a hydraulic jump may also occur when the convective mixed layer is shallower (Kodama et al., 1999) or the mountain range is higher (Kusunoki et al., 2003).

When convective cloud systems travel to the land, they experience an abrupt change of environment, such as the loss of sensible and latent heat supply and frictional convergence caused by a change of surface roughness. Moreover, hills and mountains may cause orographic updrafts and horizontal convergence. These changes in the environment may significantly change the characteristics of the convective cloud systems. Many studies of land breezes have been conducted, because of their significant effects, such as the activation of a stationary snowband (Ishihara et al., 1989; Tsuboki

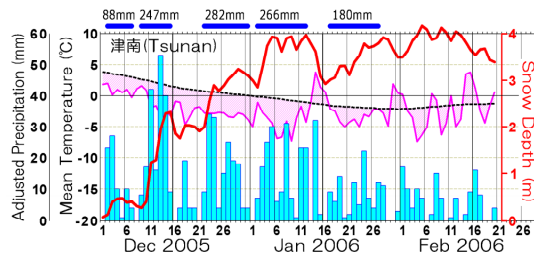


Fig. 1 Daily mean temperature ($^{\circ}\text{C}$, solid line), adjusted daily precipitation (mm, bars), and daily maximum snow depth (m, thick solid line) at the Tsunan surface meteorological station of the Japan Meteorological Agency (JMA). A black dashed line indicates the 22-year average of the daily mean temperature ($^{\circ}\text{C}$).

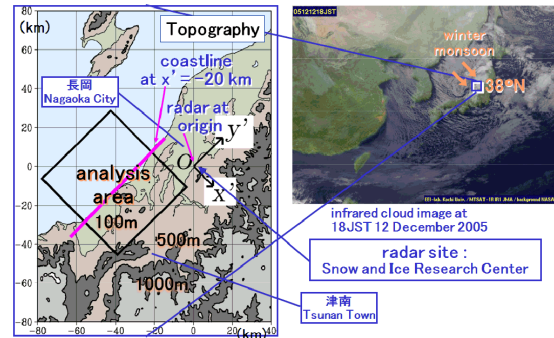


Fig. 2 (Left panel) Topography around the analysis area. O indicates the Snow and Ice Research Center (SIRC), NIED. The x' (y') axis was taken in the direction perpendicular (parallel) to the coastline. The analysis area is shown by a diagonally oriented box. (Right panel) The location of the area is shown in the left panel with a JMA MTSAT-1R infrared cloud image at 18JST December 12, 2005 (provided by Kochi University).

et al., 1989; Eito et al., 2001; Yoshihara et al., 2004; Ohigashi and Tsuboki, 2005). After Takeda et al. (1982), however, few studies have been done on changes in convective cloud systems landing within onshore monsoon winds.

Heavy snowfall brought from convective cloud systems was continuously observed associated with outbreak of a strong winter monsoon from December 2005 to February 2006. This continuous snowfall resulted in the snow depth of more than three meters among the mountains. Figure 1 is the time series of meteorological elements in Tsunan, a mountain town (Fig. 2) where many snow-related disasters (avalanches, traffic interruptions, accidents, and collapsed houses) occurred. The snowfall was brought mainly by three snowfall events with precipitation amount of more than 200



Fig. 3 A photograph of the central part of Tsunan, taken on January 10, 2006 [Photograph courtesy of Hiroyuki Hirashima, SIRC].

* Corresponding author address: Sento Nakai, Snow and Ice Research Center, NIED, Nagaoka, 940-0821 Japan; e-mail: saint@bosai.go.jp

Table 1 Classification of wintertime convective cloud systems (Nakai et al. 2005).

Longitudinal line (L-mode)	bands running or cells aligned nearly parallel to the prevailing wind
Transversal line (T-mode)	bands running or cells aligned with a large angle relative to the prevailing wind
Spreading precipitation (S-mode)	widely spreading precipitation without maintaining specific structure
Meso- β scale vortex (V-mode)	vortices and associated curved bands with a significant change of the wind direction
Mountain slope precipitation (M-mode)	a stationary precipitation area around the windward slope of the mountains
Local-frontal band (D-mode)	a wide band considered to be formed along a line of discontinuity
sub-class of the modes shown above	
Coastal intensification (xI-mode)	precipitation occasionally intensified around coastline

millimeters. The snow depth reached 4 meters, about 150% of the mean maximum snow depth, in the middle of the winter. There were high "walls" of snow in the central part of Tsunan (Fig. 3) and nearby cities even after snow was removed from the roads.

Nakai and Iwamoto (2006) reported the nationwide characteristics of snow depth distribution. Using conventional radar data, Nakai and Kumakura (2007) described general characteristics of mesoscale cloud systems. The monsoon outbreak was especially strong in December 2005, when many convective cloud systems traveled overland, giving meteorologists an opportunity to analyze the basic process of coastal effects on convective cloud systems. In this study, radar and numerical simulation data were used to examine the precipitation variations of convective cloud systems within onshore monsoon winds in relation to the coastal effect.

2. Radar Observations and Classification of Convective Cloud Systems

Radar observations were continuously carried out at the Snow and Ice Research Center (SIRC), National Research Institute for Earth Science and Disaster Prevention (NIED) (20 km from coastline, origin of Fig. 2) almost continuously from 10 to 29 December by 12-elevation volume scans in 3- to 4-minute intervals. The observed data were projected on a Cartesian coordinate with a horizontal/vertical resolution of 1 km / 500 m. The equivalent reflectivity factor (Z_e) and radial velocity (V_r) data were used for the analyses.

Thirty-three cases of convective cloud systems were identified from the radar observation data in December 2005 (Fig. 4). Among the six convective cloud systems listed in Table 1, the major systems identified in December 2005 were longitudinal lines, transversal lines, and meso-beta scale vortices. We obtained enough data to conduct statistical analyses of these three types of convective cloud systems. As the purpose of this study was to examine the variations in precipitation in a direction perpendicular to the coastline, cases with prevailing winds in a direction rather parallel to the coastline were excluded. Fourteen cases were selected for the analyses (Table 2). The number of cases and the total duration of longitudinal lines, transversal lines, and meso-beta scale vortices were, respectively, 3, 6, and 5 cases and 62.0, 75.8, and 54.9 hours.

3. Observed Variations of Precipitation Intensity

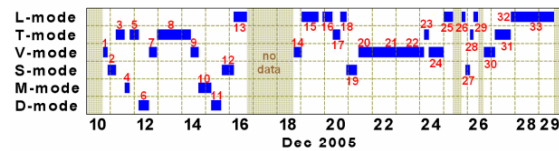


Fig. 4 Convective cloud systems observed by SIRC/NIED radar in December 2005. A numbered solid box indicates the period of a case.

The topography of the analysis area is characterized by mountains with a height of 100 to 1000 m, located about 10 to 30 km from the coastline (Fig. 2). Variations in precipitation intensity were examined with respect to the distance from the coastline. The x' - y' coordinate was defined as shown in Fig. 2. The dimensions of the diagonal box in Fig. 2 are 55 and 50 km in the x' and y' directions, respectively. The x' - and y' -axes are nearly perpendicular and parallel to the coastline, respectively. The line of $x'=-20$ km almost corresponds to the coastline. The observation data were reprojected on the x' - y' coordinate, and the following analysis was performed using the data within the diagonal box. The precipitation variation was investigated using the snow water equivalent (SWE), which was calculated assuming a Ze-SWE relation derived using the formulae of Fujiyoshi et al. (1990), Gunn and Marshall (1958), and Langbein (1954).

Figure 5a shows the time- x' cross section of precipitation variations for the longitudinal lines in case 33, using the snow water equivalent (SWE) amount at a height of 1500 m. Note that the cross

Table 2 Characteristics of the 14 cases of convective cloud systems. A start or end time given in parentheses indicates that the observation period was discontinued. ∇ SWE indicates the SWE gradient in the direction perpendicular to the coastline.

case#	start (day,time)	end (day,time)	classification	prevailing wind 1500 m ASL	duration (hour)	∇ SWE _{sea} ($\text{mg m}^{-3} \text{km}^{-1}$)	∇ SWE _{land} ($\text{mg m}^{-3} \text{km}^{-1}$)
15	19.0043JST	19.1744JST	L	WNW	17.0	1.8	1.9
29	26.0552JST	(26.1044JST)	L	WNW	4.9	-0.4	4.7
33	27.2303JST	(29.1509)JST	L	WNW	40.1	0.5	1.5
3	11.0526JST	11.1411JST	T	NW	8.8	1.4	6.7
5	11.1919JST	12.0420JST	T	NW	9.0	1.7	2.4
8	12.2257JST	14.0851JST	T	NW	33.9	0.9	5.5
23	24.0408JST	24.0855JST	T	NW	4.8	1.7	8.6
28	26.0223JST	26.0548JST	T	WNW	3.4	2.8	5.1
31	27.0337JST	27.1935JST	T	NW	16.0	1.4	4.7
1	(10.1623)JST	10.2100JST	V	W<->NW	4.6	2.0	3.4
7	12.1447JST	12.2254JST	V	SW->NW	8.1	3.4	-3.3
21	22.1928JST	23.1126JST	V	W->WNW	16.0	-1.2	3.0
24	24.0856JST	25.0004JST	V	WNW->NW->W	15.1	3.0	-0.1
30	(26.1626)JST	27.0333JST	V	WNW	11.1	0.5	2.2

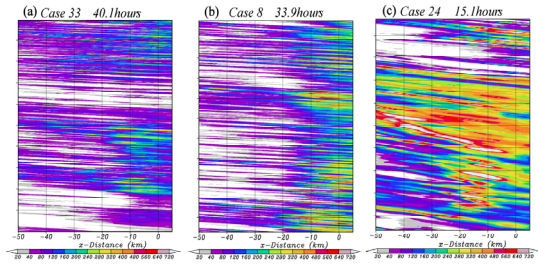


Fig. 5 Time- x' cross section of the radar-based SWE averaged in y' direction in the diagonal box in Fig. 2 at a height of 1500 m. (a) Case 33 (longitudinal lines), (b) case 5 (transversal lines), and (c) case 24 (meso-beta scale vortices). The coastline is located at $x'=-20$ km. The colored bar indicates the y' -mean SWE (10^3 g m $^{-2}$)

section shows the SWE averaged for a length of 50 km in the y' direction. An area with a large SWE indicates the existence of groups of cells with a scale of about 20 km, but not a convective cell. The precipitation areas continuously moved to the positive x' direction across the coastline to the inland. Moreover, the increase in the SWE was superimposed on this movement. The other two cases of longitudinal lines (see Table 2) were also analyzed. The x' -variation of SWE was averaged for the period of each case (Fig. 6). All three cases of longitudinal lines showed a change in the SWE gradient in the x' direction at the coastline. The radar echo-top height, defined by $Z_e=12$ dBZ, was derived from the three-dimensional Z_e distribution. To eliminate ground clutter and low-level fragmental precipitation, the echo-top height was neglected when it was lower than 2500 m. Time- x' cross section of echo-top heights averaged for a 50 km length in the y' -direction is shown in Fig. 7. For the longitudinal lines in case 33, the echo top height slightly increases from the coastline to the inland, although the maximum SWE at a 1500 m height is found farther about 10 km inland, where the echo top decreases to about 3000 m.

These characteristics were confirmed by a vertical cross section of SWE in the x' direction (Fig. 8a). The convective cloud system has the maximum height near $x'=-10$ km (10 km inland from the coastline). The maximum SWE is found 20 km inland from the coastline at the lowest analysis level (500m), where the SWE increases twice in comparison with that over the sea (Fig. 8a). The SWE on the land becomes smaller with altitude. The SWE over the sea had downward-positive vertical gradient at all levels, although it is smaller than that on the land. The SWE in the layer lower than 2000 m increases from $x'=-50$ km to $x'=-30$ km (30km and 10km offshore, respectively).

Similar characteristics are found in the SWE vertical sections of other longitudinal-line cases. Case 29 showed an SWE minimum 5 km offshore in a time- x' cross section, and the vertical section of the mean SWE clearly indicated the corresponding minimum at $x'=-25$ km (not shown). An SWE increase over the sea, found in case 33 (Fig. 8a) seems to be discontinued to another increase of SWE on the land. These facts suggest that two precipitation enhance mechanisms, one

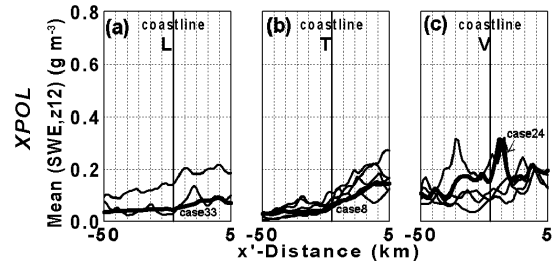


Fig. 6 Variations in the radar-based SWE with respect to the x' -distance (abscissa) averaged in the y' direction of the analysis area and in the period of each case. (a) Longitudinal lines (L), (b) transversal lines (T), and (c) meso-beta scale vortices (V). The cases shown in Fig. 5 are indicated by case numbers.

over the sea and the other on the land, coexist in these longitudinal lines of convection.

Figure 5b is the time- x' cross section of precipitation variations for the transversal lines in case 8. The precipitation areas continuously moved in a positive x' direction across the coastline to the inland. The increase in the SWE was also superimposed on the southeastward movement of the precipitation areas. However, the amount of enhancement was significant, unlike that in the cases of longitudinal lines. All six cases of transversal lines show significant SWE increase in the x' direction on the land (Fig. 6b). In case 8, the echo-top height abruptly increased from lower than 2500 m to 4000 m at the coastline and then maintained the highest level on the land (Fig. 7b), although the SWE at a 1500-m height continued to increase to 25 km inland from the coastline (Fig. 5b).

These characteristics are confirmed by an x' -vertical cross section of SWE (Fig. 8b). The height of the convective cloud system increased on the land from $x'=-20$ km to $x'=-10$ km and then maintained the height. The maximum SWE is found at the edge of the analysis area (25 km inland from the coastline) at the lowest analysis level (500m), where the SWE increases four times in comparison with that over the sea (Fig. 8b). The SWE on the land becomes smaller with altitude. The SWE over the sea smoothly increases to the coastline, although the increase rate is smaller than that on the land. Similar characteristics were found in the SWE vertical sections of other transversal-line cases. No case of transversal lines showed an SWE minimum over the sea (not shown).

The precipitation variation of transversal lines

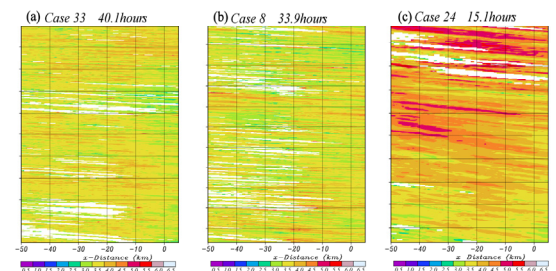


Fig. 7 Same as Fig. 5, but for the echo-top height defined by $Z_e=12$ dBZ.

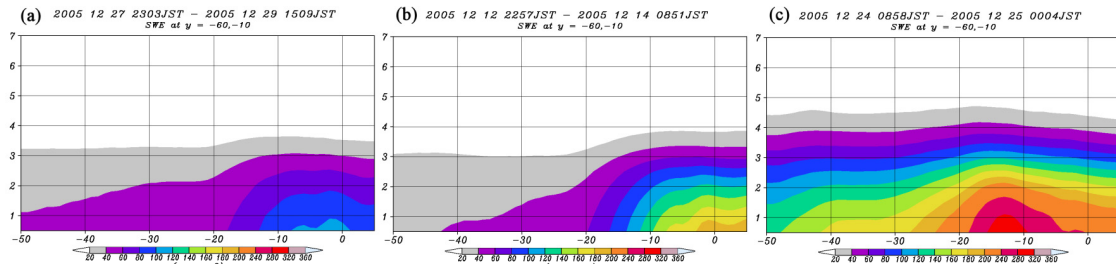


Fig. 8 Vertical section of the y' -mean of the case-mean radar-based SWE (10^{-3} g m^{-3}) shown in the diagonal box in Fig. 2. The abscissa is x' (km) and the ordinate is height (km). (a) Case 33 (longitudinal lines), (b) case 5 (transversal lines), (c) case 24 (meso-beta scale vortices). The coastline is located at $x'=-20$ km.

is qualitatively similar but quantitatively different from that of longitudinal lines. Both of them have large SWE increase in the x' direction on the land than over the sea (Table 2). However, transversal lines showed a larger SWE increase rate over the land. The cause of the difference could be attributed to 1) the inherent difference in the structure of convective cloud systems or 2) the interaction between the differently oriented convective cloud systems and the coastal topography. To clarify this point, a detailed three-dimensional analysis and a numerical study are necessary.

Figure 5c shows the time- x' cross section of for the meso-beta scale vortices in case 24. The precipitation areas moved in a positive x' direction across the coastline to the inland. The traveling speed was not constant as seen in cases 33 and 8. The meso-beta scale vortices are often organized as a train of vortices (e.g. Nagata, 1993) or a multi-scale vortex family (Ninomiya and Hoshino, 1990). The cloud system of the case 24 was a group of vortex trains organized in approximately 400 km scale with a counterclockwise rotating motion. The motion of individual clouds in the analysis area was affected by that of the whole cloud system, resulting in the fluctuation of the motion found in Fig. 5c. The maximum of SWE in case 24 is found at $x'=-15$ km (5 km inland from the coastline).

Other four cases of meso-beta scale vortices (see Table 2) were also analyzed. The x' -variation of SWE was averaged for the period of each case (Fig. 6c). No case showed a significant increase in SWE, and the variations in the x' -direction were different from each other. The difference could be brought from the meso-alpha scale motion that contained the vortices found in the analysis area.

The echo-top height of 5000 m or more was observed at far offshore from the coastline during

the period of case 24 (Fig. 7c). The echo-top height sometimes slightly increased toward the coastline, while it decreased gradually after the precipitating cloud landed. The x' -vertical cross section of the y' -mean SWE of case 24 is shown in Fig. 8c. The height of the convective cloud system little changes over the sea and decreases on the land with the maximum at $x'=-15$ km (5 km inland). The SWE increase was clear on the land below a height of 3000 m. This vertical contrast was common characteristics of five meso-beta scale vortices cases. The SWE increases over the sea and near the coast, and the maximum SWE is found at $x'=-12$ km (8 km inland from the coastline) at the lowest analysis level (500m) in case 24. In all cases of meso-beta scale vortices, the location of the maximum SWE did not appear in the inland areas ($x'>-10$), although the locations were different among the cases.

4. Reproduced Precipitation by Numerical Simulations

A numerical simulation experiment of snowfall in December 2005 was carried out at the Meteorological Research Institute (MRI) through the double nesting of JMANHM. JMANHM is a nonhydrostatic mesoscale model for research and operational use developed at the Numerical Prediction Division (NPD) of the Japan Meteorological Agency (JMA) and the MRI. Details of the JMANHM are described in Saito et al. (2006).

The simulation was started every 6 hours. The outer model was executed using regional objective analysis data (RANAL) of JMA as initial and boundary conditions. The 3-hour forecast and the succeeding forecast data of the outer model were used as the initial and boundary conditions of the inner model. The horizontal resolutions of the

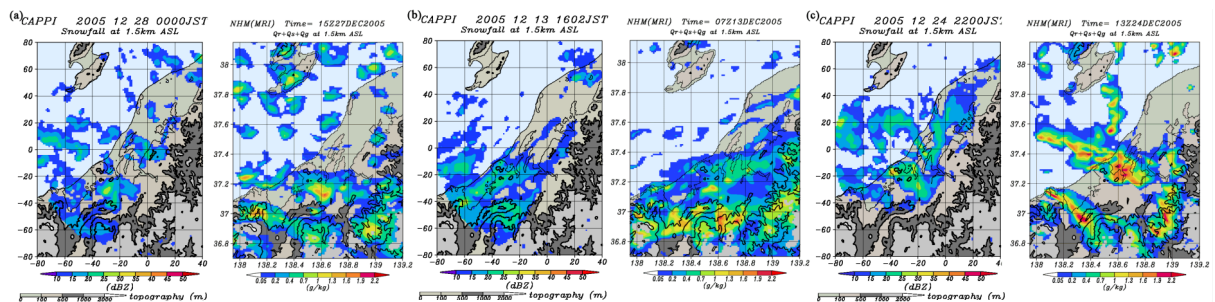


Fig. 9 Examples of the radar-model snapshot comparison of snowfall distribution at a height of 1500 m. (a) Longitudinal lines (L), (b) transversal lines (T), and (c) meso-beta scale vortices (V).

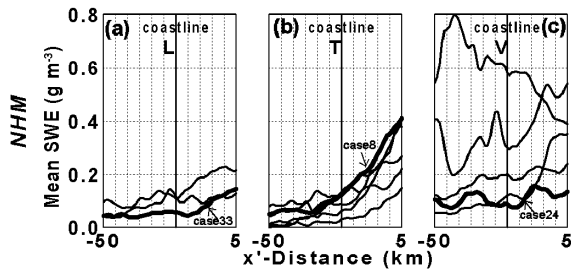


Fig. 10 Same as Fig. 6, but for the simulated SWE.

RANAL, outer and inner models are 10 km, 5 km, and 1 km, respectively. An explicit 2-moment bulk-type cloud microphysics scheme (Ikawa and Saito 1991) was used in both the outer and inner models. The Kain-Fritsch convective parameterization scheme (Kain and Fritsch 1993) was additionally applied only to the outer model. The integration time of the inner model was nine hours and the data output interval was 1 hour in the forecast time. Four-hour to nine-hour forecast data were used for the following analysis.

The aim of this section is to compare the simulation data with the radar observation data described in the previous section. A partial data set, covering only the observation range of the radar, was made to facilitate the analysis. The area of the partial data set is sufficiently far from the inner model boundary.

Figure 9 shows examples of the snapshot of the radar precipitation intensity at a height of 1500 m and the corresponding total mixing ratio of precipitation particles (rain, snow and graupel), Q_p , simulated by the inner model. The linear features of the longitudinal and transversal lines were well simulated (Figs. 9a and 9b). The running direction of the simulated lines was well simulated in cases of longitudinal lines, while it was often slightly different from the observations in cases of transversal lines. In cases of meso-beta scale vortices, the precipitation features of curved lines and vortices were reproduced in three of the five cases. An example of the reproduced curved lines is shown in Fig. 9c. The numerical simulation reproduced double curved lines although the detailed structure was different.

The SWE was calculated from simulated Q_p and was compared with the observed SWE on the x' - y' coordinate. The x' -variation of the simulated SWE was averaged for the period of each case. Figure 10a shows the simulated precipitation variation in the x' direction for the three cases of longitudinal lines. All cases show the rapid

increase of the simulated SWE around the coastline. The x' gradient of the simulated SWE on the land was larger than that over the sea. Figure 10b shows the precipitation variations for the six cases of transversal lines. The significant precipitation enhancement on the land (Fig. 6b) was reproduced in all six cases, which is the major different feature between transversal and longitudinal lines.

As shown in Figs. 10a and 10b, the qualitative performance of the simulation of the linear-shaped precipitation systems near the coastal topography is good. The simulated SWE on the land for case 8 (Fig. 10b) is the largest among six cases of transversal lines, while the radar-based SWE of case 8 (Fig. 6b) is relatively small. The quantitative correspondence of the simulated SWE with the radar-based SWE may not be sufficient, however, a different approach, such as an analysis of the three-dimensional structure of a snapshot, may be necessary for the quantitative comparison.

Figure 10c shows the simulated precipitation variations for the meso-beta scale vortex cases. The linear increase in the x' direction is not clear in the SWE variations, and a few maxima are found. This feature is similar to the radar-based SWE. The simulated SWE for case 24 has a maximum at $x' = -10$ km and $x' = -35$ km corresponding to the maxima of the radar-based SWE at $x' = -15$ km and $x' = -30$ km, respectively. However, the amplitude of the simulated SWE variation is larger than that of the radar-based SWE. This could be brought from the difference in the Ze-SWE relation between longitudinal/transversal lines and meso-beta scale vortices. The prevailing snow particles of longitudinal/transversal lines are graupels, while those of the meso-beta scale vortices are rimed snowflakes. The Ze-SWE relation used in our analysis may be suitable for snowfall particles of longitudinal/transversal lines. The radar-based SWE may be underestimated because of the mismatch of the Ze-SWE relation and snowfall particles, especially for snowfall particles of meso-beta scale vortices.

The characteristics of the precipitation variations in the x' direction were qualitatively well reproduced in the numerical simulation. Especially, the differences among longitudinal lines, transversal lines, and meso-beta scale vortices were clear as the results from the radar data. The numerical simulation confirmed that the variation in precipitation intensity around the coastal topography depends on the type of convective cloud systems.

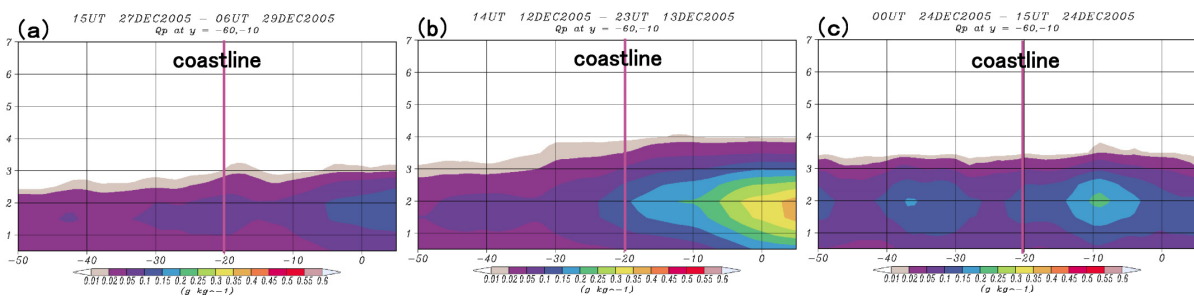


Fig. 11 Same as Fig. 8, but for the simulated Q_p (g kg^{-1}).

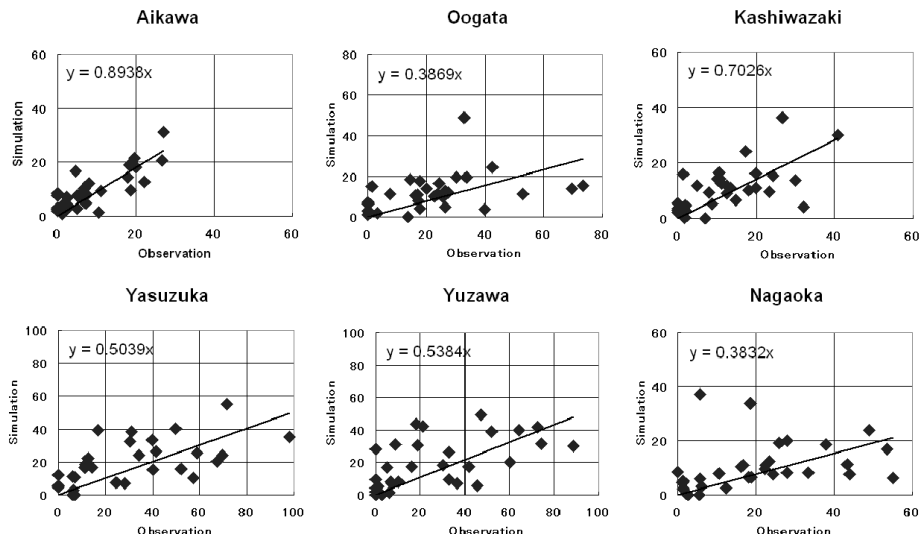


Fig. 12 Comparison of daily precipitation (mm) between observations (abscissa) and simulations (ordinate) in December 2005 at six JMA surface meteorological stations.

Figure 11 shows the vertical cross section of the simulated Q_p of the same cases shown in Fig. 8. The characteristics of the precipitation variation in the x' direction were well simulated especially above a height of 1500 m. The vertical gradient of the simulated Q_p in all cases was opposite to the radar-based SWE, i.e., downward-negative below 1500 m.

The simulated surface precipitation was compared with the surface raingauge data. The comparison was made using daily precipitation data from 1 to 31 December 2005 at the six AMeDAS stations around the analysis area shown in Fig. 2. The surface precipitation amount was adjusted for wind loss (Goodison et al. 1998) using the formula of Yokoyama et al. (2003). The regression coefficient of the simulated precipitation to the adjusted precipitation ranged from 0.38 to 0.89 (Fig. 12). The six-point average of the regression coefficient was 0.57, indicating a significant underestimation of the simulated precipitation.

Figure 13 is the comparison of hourly surface relative humidity between the simulation and surface observation at Niigata and SIRC. The relative humidity around 60% was well simulated, though the observed high relative humidity (>80%) was not sufficiently reproduced at Niigata. High relative humidity was more frequently observed at SIRC. Therefore, the relative humidity tends to be underestimated in the simulation. The numerical experiment produced a drier environment at the low level, especially in inland areas. This suggests that more snow particles below a height of 1500 m evaporated in the dry environment to result in the underestimation of the surface precipitation.

5. Summary

The effect of coastal topography on the precipitation of convective cloud systems was examined by radar observation and numerical simulation. The observed and simulated precipitation variation showed qualitatively similar

characteristics. The simulation successfully reproduced the features of precipitating cloud systems.

Variations in snowfall intensity were examined based on radar observations for the convective systems, with respect to the distance from the coastline. The analysis was performed for fourteen cases with northwesterly or north-northwesterly prevailing winds.

The cases were classified as three types of convective cloud systems: longitudinal lines, transversal lines, and meso-beta scale vortices. The precipitation variations among the three types showed different characteristics. The precipitation intensity for longitudinal lines moderately enhanced on the land. For transversal lines, the enhancement on the land was more significant. The difference between longitudinal and transversal lines was outstanding in spite of their similarity in the linearly extended shape of precipitation areas. These features can be brought from the structure of the convective systems and the effect of the coastal topography. The precipitation variation for meso-beta scale vortices was characterized by a low-level SWE maximum and an echo-top maximum found around the coastal area. The numerical simulation confirmed

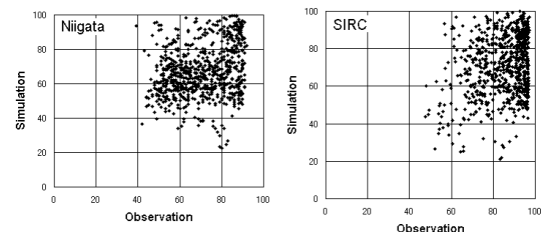


Fig. 13 Comparison of hourly relative humidity (%) between observations (abscissa) and simulations (ordinate) in December 2005 at the Niigata Local Observatory, JMA and SIRC.

that the variation in precipitation intensity around the coastal topography depends on the type of convective cloud systems.

The numerical simulation showed different characteristics in vertical cross sections of the case-mean SWE. The precipitation weakened toward the surface below a height of 1500 m, in all longitudinal/transversal lines and meso-beta scale vortices. The difference could be brought from the evaporation of falling snow particles in unrealistic simulated dry environment at the low levels. The evaporation also caused the underestimation of the surface precipitation.

The simulated relative humidity at the low level should be improved appropriately by examining the parameters related to the surface processes and/or the cloud microphysics. The environmental conditions favorable to a specific type of convective cloud systems, and their detailed structure, particularly the difference among the three types, are also the topics to be clarified in the future issues.

Acknowledgments

This work is supported by a projects of the National Research Institute for Earth Science and Disaster Prevention titled "Research project for developing a snow disaster forecasting system and snow hazard maps." GrADS (Grid Analysis and Display System) was used to draw some of the figures.

References

- Eito, H., T. Kato, M. Yoshizaki and A. Adachi, 2001: Numerical simulation of the quasi-stationary snowband observed over the southern coastal area of the Sea of Japan on 16 January 2001. *J. Meteor. Soc. Japan*, 83, 551-576.
- Fujiyoshi, Y., T. Endoh, T. Yamada, K. Tsuboki, Y. Tachibana and G. Wakahama, 1990: Determination of a Z-R relationship for snowfall using a radar and high sensitivity snow gauges. *J. Atmos. Sci.*, 29, 147-152.
- Goodison, B. E., P. Y. T. Louie, and D. Yang, 1998: WMO Solid Precipitation Measurement Intercomparison, Final Report. WMO/TD-No. 872, Instruments and Observing Methods Report No. 67, 212pp.
- Gunn, K. L. S. and J. S. Marshall, 1958: The distribution with size of aggregate snowflakes. *J. Meteor.*, 16, 452-461.
- Ikawa, M., and K. Saito, 1991: Description of a non-hydrostatic model developed at the Forecast Research Department of the MRI. MRI Tech. Rep. 28, 238 pp.
- Ishihara, M., H. Sakakibara and Z. Yanagisawa, 1989: Doppler radar analysis of the structure of mesoscale snow bands developed between the winter monsoon and the land breeze. *J. Meteor. Soc. Japan*, 67, 503 - 520.
- Kain, J. and J. Fritsch, 1993: Convective parameterization for mesoscale models: The Kain-Fritsch scheme. The Representation of Cumulus Convection in Numerical Models, Meteor. Monogr., No. 46, Amer. Meteor. Soc., 165-170.
- Kodama, Y.-M., M. Maki, S. Ando, M. Otsuki, O. Inaba, J. Inoue, N. Koshimae, S. Nakai and T. Yagi, 1999: A weak-wind zone accompanied with swelled snow clouds in the upstream of a low-altitude ridge - Single Doppler radar observations over the Tsugaru District of Japan - , *J. Meteor. Soc. Japan*, 77, 1039-1059.
- Kusunoki, K., M. Murakami, N. Orikasa, Y. Tanaka, K. Iwanami, M. Maki, S.-G. Park, R. Misumi, K. Hamazu and H. Kosuge, 2003: Ka-band radar observations of orographic snow clouds and flows across a steep mountain ridge. 31st International Conference on Radar Meteorology, 6-12 August 2003, Seattle, USA, 104-107.
- Langleben, M. P., 1954: The terminal velocity of snowflakes. *Quart. J. Roy. Meteor. Soc.*, 80, 174.
- Nagata, M., 1993: Meso- β scale vortices developing along the Japan-Sea polar-airmass convergence zone (JPCZ) cloud band: Numerical simulation. *J. Meteor. Soc. Japan*, 71, 43-57.
- Nakai, S. and T. Endoh, 1995: Observation of snowfall and airflow over a low mountain barrier. *J. Meteor. Soc. Japan*, 73, 183-199.
- Nakai, S., K. Iwanami, R. Misumi, S.-G. Park and T. Kobayashi, 2005: A classification of snow clouds by Doppler radar observations at Nagaoka, Japan. *SOLA*, 1, 161-164.
- Nakai, S. and K. Iwamoto, 2006: Characteristics of the heavy snow of the 2006 winter season in Japan indicated by the normalized maximum snow depth. *Tenki*, 53, 863-869 (in Japanese with English abstract and figures).
- Nakai, S. and T. Kumakura, 2007: Snowfall distribution characteristics of the heavy snow of the 2005/2006 Japanese winter: An analysis of the radar data of 3 months in 10-minute intervals. *Seppyo*, 69, 31-43 (in Japanese with English abstract).
- Ninomiya, K. and K. Hoshino, 1990: Evolution process and multi-scale structure of a polar low developed over the Japan Sea on 11-12 December 1985 Part II: Meso- β -scale low in meso- α -scale polar low. *J. Meteor. Soc. Japan*, 68, 307-318.
- Ohigashi, T. and K. Tsuboki, 2005: Structure and maintenance process of stationary double snowbands along the coastal region. *J. Meteor. Soc. Japan*, 83.
- Saito, K., T. Fujita, Y. Yamada, J. Ishida, Y. Kumagai, K. Aranami, S. Ohmori, R. Nagasawa, S. Kumagai, C. Muroi, T. Kato, H. Eito and Y. Yamazaki, 2006: The operational JMA nonhydrostatic mesoscale model. *Mon. Wea. Rev.*, 134, 1266-1298.
- Takeda, T., K. Isono, M. Wada, Y. Ishizaka, K. Okada, Y. Fujiyoshi, M. Maruyama, Y. Izawa and K. Nagaya, 1982: Modification of convective snow - clouds in landing the Japan Sea coastal region. *J. Meteor. Soc. Japan*, 60, 967-977.
- Tsuboki, K., Y. Fujiyoshi and G. Wakahama, 1989: Doppler radar observation of convergence band cloud formed on the west coast of Hokkaido Island. II: cold frontal type. *J. Meteor. Soc. Japan*, 67, 985-999.
- Yokoyama, K., H. Ohno, Y. Kominami, S. Inoue

and T. Kawakata, 2003: Performance of Japanese precipitation gauges in winter. *Seppyo*, 65, 303-316 (in Japanese with English abstract and figures).
Yoshihara, H., M. Kawashima, K. Arai, J. Inoue

and Y. Fujiyoshi, 2004: Doppler radar study on the successive development of snowbands at a convergence line near the coastal region of Hokuriku District. *J. Meteor. Soc. Japan*, 82, 1057-1079.